Multistage construction of Gd-Doped g-C_3N_4/$Mo_{15}S_{19}$ Composites Enabled Both N_2 activation and multiple electron transfer for Enhanced Photocatalytic Nitrogen Reduction Reaction

Xiaoyu Jiang,[a,b] Boran Tao,[c] Hongda Li[a,b,*]

[a] School of Chemistry and Chemical Engineering, Hubei Normal University, Huangshi 435002, China

[b] Suzhou Institute for Advanced Research, University of Science and Technology of China, Suzhou 215123, China

[c] Tianmu Lake Institute of Advanced Energy Storage Technologies Co., Ltd., Liyang 213300, China

Corresponding author: Hongda Li, hdli@ustc.edu.cn

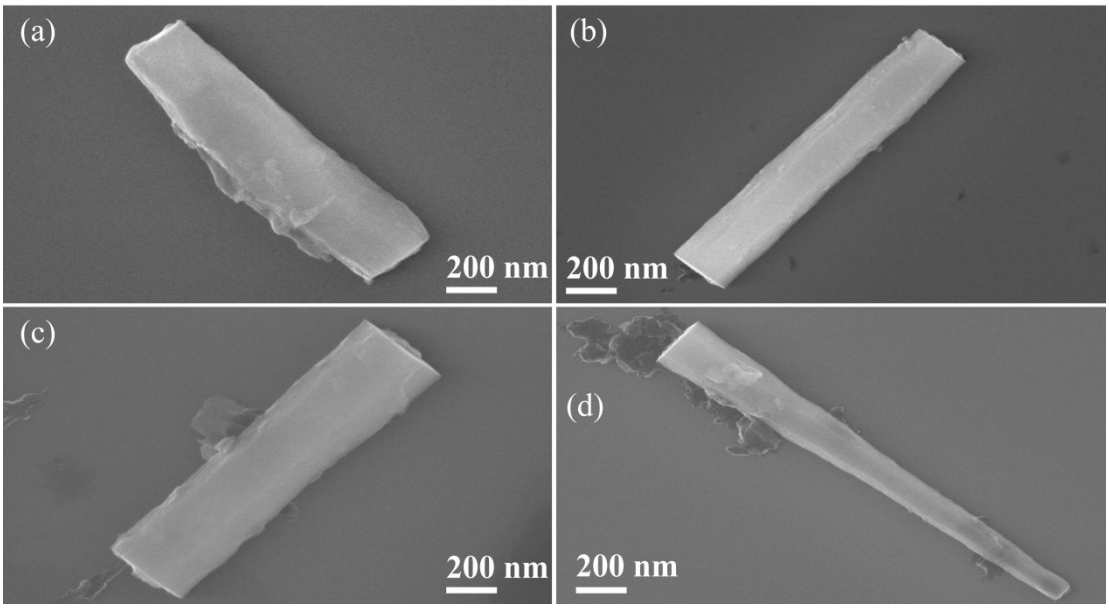

Fig. S1. SEM images of (a) C_3N_4, (b) GdC_3N_4, (c) $GdC_3N_4/Mo_{15}S_{19}$, and (d) $C_3N_4/Mo_{15}S_{19}$

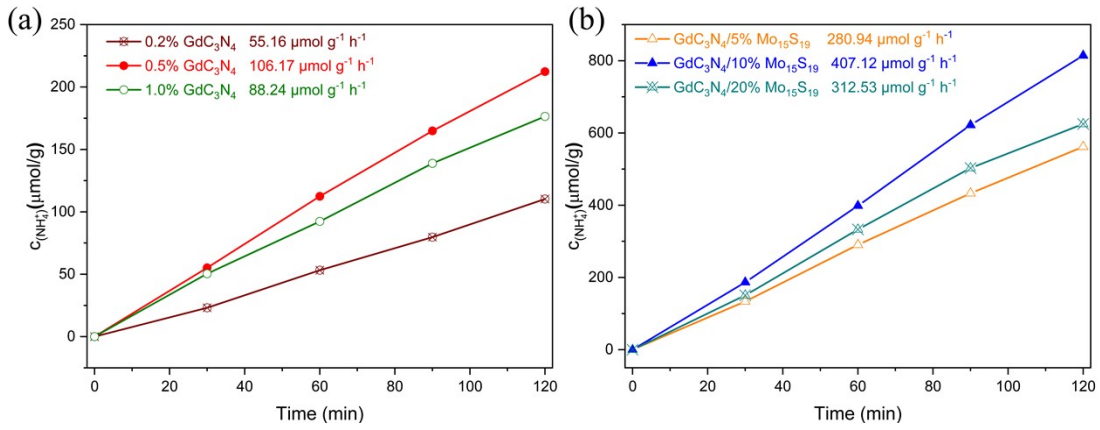

Fig. S2. (a) Photocatalytic NRR of 0.2% GdC_3N_4, 0.5% GdC_3N_4, 1.0% GdC_3N_4 under visible light irradiation; (b) Photocatalytic NRR of GdC_3N_4/5% $Mo_{15}S_{19}$, GdC_3N_4/10% $Mo_{15}S_{19}$, GdC_3N_4/20% $Mo_{15}S_{19}$ under visible light irradiation

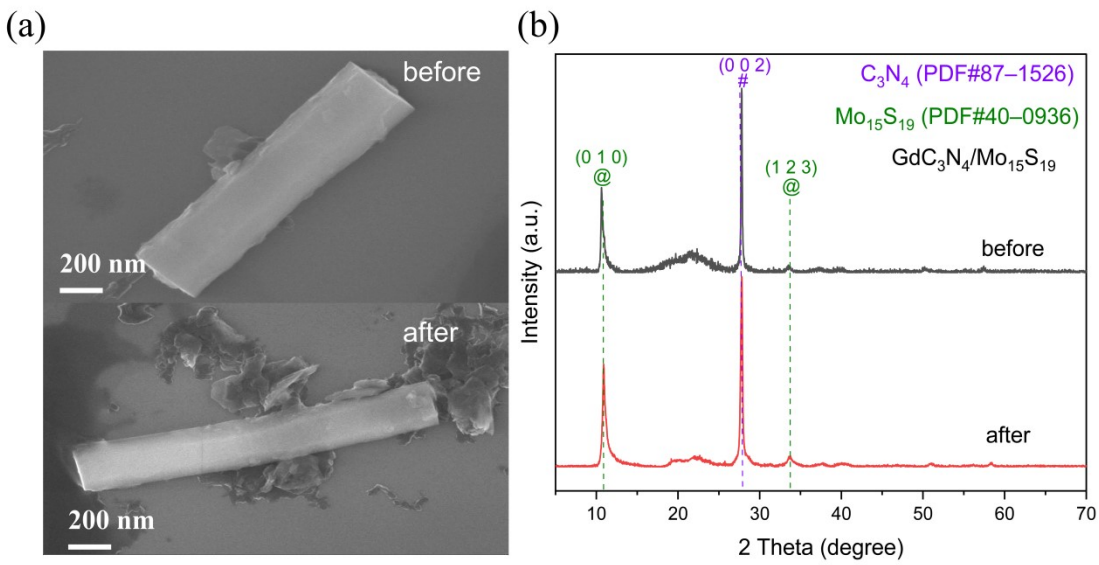

Fig. S3. (a) SEM images and (b) XRD patterns of $GdC_3N_4/Mo_{15}S_{19}$ samples before and after the reaction (four cycles).

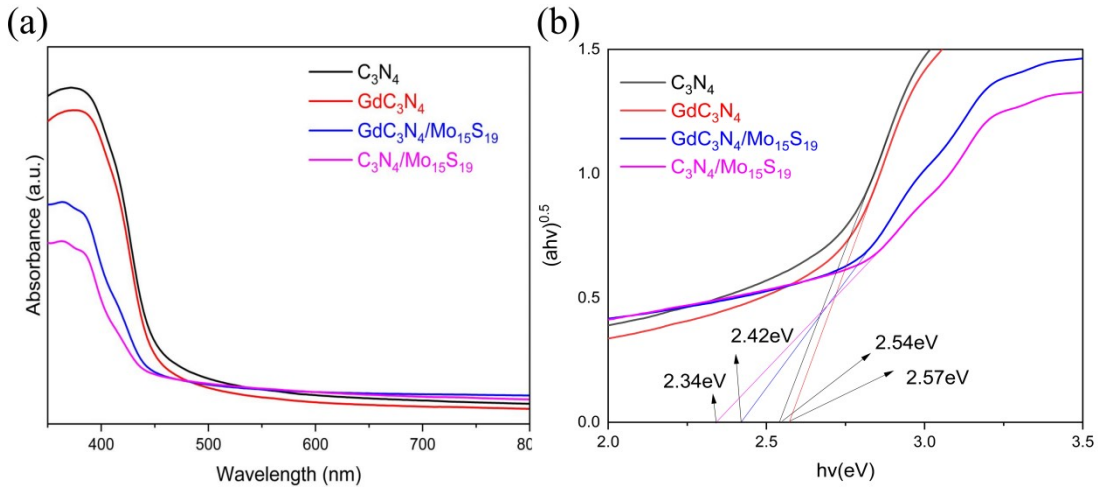

Fig. S4. (a) UV–vis diffuse reflectance spectra (DRS) of g-C_3N_4, GdC_3N_4, $GdC_3N_4/Mo_{15}S_{19}$, and $C_3N_4/Mo_{15}S_{19}$. (b) Band gap values of g-C_3N_4, GdC_3N_4, $GdC_3N_4/Mo_{15}S_{19}$, and $C_3N_4/Mo_{15}S_{19}$. The bandgap calculation formula is given by: $(\alpha h\nu)^{1/2}=A(h\nu-Eg)$, in which A, *h*, ν, α, and Eg represent the proportionality constant, Planck's constant, absorption coefficient, light frequency, and bandgap energy, respectively.

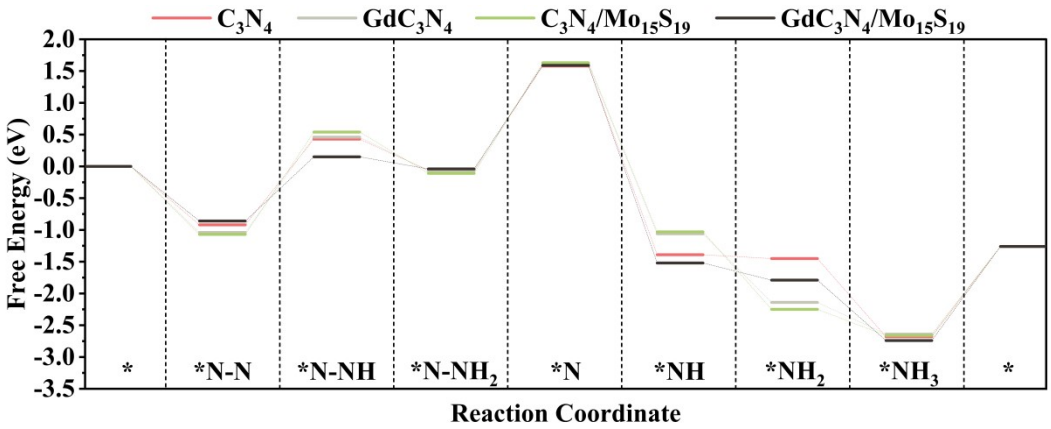

Fig. S5. Gibbs free energy profiles of the distal mechanism for the NRR process on the g-C_3N_4, GdC_3N_4, $GdC_3N_4/Mo_{15}S_{19}$, and $C_3N_4/Mo_{15}S_{19}$ catalysts.

Table S1. Element concentrations by Energy dispersive spectrometer (EDS), BET specific surface areas of g-C_3N_4, GdC_3N_4, $GdC_3N_4/Mo_{15}S_{19}$ and $C_3N_4/Mo_{15}S_{19}$.

Samples	**g-C_3N_4**	**GdC_3N_4**	**$GdC_3N_4/Mo_{15}S_{19}$**	**$C_3N_4/Mo_{15}S_{19}$**
Surface areas (m^2 g^{-1})	16.16	17.25	42.13	42.30
C Mass%	72.11	71.66	64.58	65.03
N Mass%	27.89	27.86	25.13	25.44
Gd Mass%	/	0.48	0.42	/
Mo Mass%	/	/	6.92	6.72
S Mass%	/	/	2.95	2.81
Real Gd (wt.%, Gd/C_3N_4)	/	0.48	0.47	/
Real Mo/S (at.%)	/	/	15.00:19.18	15.00:18.81
Real $Mo_{15}S_{19}$ (wt.%)	/	/	9.87	9.53

Table S2. The adsorption energies of N_2 on Mo, S, N, C, and Gd sites

Site	**Adsorption Energy (eV)**
Mo	-0.92
Gd	-0.87
N	-0.75
C	-0.69
S	-0.63

Table S3. Photocatalytic nitrogen fixation performance of different catalysts under various reaction conditions.

Catalysts	Scavenger	Light Source	NH_3 generation rate $\mu mol\ g^{-1}\ h^{-1}$	Ref.
S-doped Bi_2MoO_6	None	300 W Xe lamp, λ>420 nm	122.14	S1
5% Cu/$InVO_4$	None	300 W Xe lamp	195.11	S2
$BiVO_4$/VS-MoS_2	None	300 W Xe lamp	132.8	S3
IL-TiO_{2-x}	Methanol	300 W Xe lamp	22.7	S4
MoS_2/In-Bi_2MoO_6	None	300 W Xe lamp	90	S5
BiOBr/g-C_3N_4	None	300 W Xe lamp	164.69	S6
Ru_1/TiO_2-Vo	None	300 W Xe lamp	18.9	S7
Gd-Bi_2MoO_6	None	300 W Xe lamp, λ>420 nm	300.15	S8
CdS/WO_3	None	300 W Xe lamp	35.8	S9
Ni_2P-BP	Methanol	300 W Xe lamp, λ>420 nm	6.14	S10
$GdC_3N_4/Mo_{15}S_{19}$	None	300 W Xe lamp, λ>420 nm	407.51	This work

References

S1 Z. Liu, M. Luo, Y. Cao, L. Meng, Y. Yang and X. Li, Tuning the electronic properties of Bi_2MoO_6 by S-doping to boost efficient photocatalytic nitrogen fixation reactions. *J. Catal.* 2024, **430**, 115347.

S2 S. Yao, J. Lin, K. Yi, W. Liu, and M. Wang, Cu-modified $InVO_4$ photocatalysts for enhanced N_2 fixation using chemical reagents and electroplating sludge as the Cu source. *Chem. Commun*. 2024, **60**, 1790.

S3 H. Luo, Z. Liu, M. Zhang, Y. Mu and M. Zhang, Construction of a $BiVO_4$/VS-MoS_2 S-scheme heterojunction for efficient photocatalytic nitrogen fixation. *Nanoscale Adv.*, 2024, **6**, 1781.

S4 X. Gong, B. Chong, M. Xia, H. Li, H. Ou, and G. Yang, Fluorinated phosphonium ionic liquid boosts the N_2-adsorbing ability of TiO_2 for efficient photocatalytic NH_3 synthesis. *Catal. Sci. Technol.* 2024, **14**, 343.

S5 T. Ma, R. Li, Y. C. Huang, Y. Lu, L. Guo, M. Niu, X. Huang, R. A. Soomro, J. Ren, Q. Wang, B. Xu, C. Yang, F. Fu and D. Wang, Interfacial Chemical-Bonded MoS_2/In-Bi_2MoO_6 Heterostructure for Enhanced Photocatalytic Nitrogen-to-Ammonia Conversion. *ACS Catal.* 2024, **14**(8), 6292-6304.

S6 L. Zhang, M. Jiang, H. Tian, S. Liu, X. Zhou, H. Liu, S. Gan, S. Che, Z. Chen, Y. Li, T. Wang, G. Wang and C. Wang, Oxygen and Nitrogen Vacancies in a BiOBr/g-C_3N_4 Heterojunction for Sustainable Solar Ammonia Fertilizer Synthesis. *ACS Sus. Chem. Eng.* 2024, **12**(5), 2028-2040.

S7 G. Ren, M. Shi, S. Liu, Z. Li, Z. Zhang and X. Meng, Molecular-level insight into photocatalytic reduction of N_2 over Ruthenium single atom modified TiO_2 by electronic Metal-support interaction. *Chem. Eng. J.* 2023, **454**, 140158.

S8 H. Li, H. Zhao, C. Li, B. Li, B. Tao, S. Gu, G. Wang and H. Chang, Redox regulation of photocatalytic nitrogen reduction reaction by gadolinium doping in two-dimensional bismuth molybdate nanosheets. *Appl. Surf. Sci.* 2022, **600**, 154105.

S9 P. Xia, X. Pan, S. Jiang, J. Yu, B. He, P. M. Ismail, W. Bai, J. Yang, L. Yang, H. Zhang, M. Cheng, H. Li, Q. Zhang, C. Xiao and Y. Xie, Designing a Redox Heterojunction for Photocatalytic "Overall Nitrogen Fixation" under Mild Conditions. *Adv. Mater.* 2022, **34**, 2200563.

S10 Z.-K. Shen, Y. Jin, X. Zhang, J. Wu, H. Wang, and Z. Huang, Identifying the role of interface

chemical bonds in activating charge transfer for enhanced photocatalytic nitrogen fixation of Ni_2P-black phosphorus photocatalysts. *Appl. Catal. B: Environ.* 2021, **295**, 120274.